Nutrient subsidies restructure coral reef dissolved carbon fluxes via biogeochemical cascades

Nyssa Silbiger (nyssa.silbiger@csun.edu)
California State University, Northridge https://orcid.org/0000-0003-4916-3217
Megan Donahue
Benjamin Hagedorn
Danielle Barnas
Hendrikje Jorissen
Jamie Kerlin
Rayna McClintock
Emily Nixon
Wesley Sparagon
Maya Zeff
Craig Nelson

Article

Keywords: Submarine groundwater discharge, ecosystem metabolism, biogeochemical cascade, allochthonous inputs

Posted Date: July 3rd, 2023

DOI: https://doi.org/10.21203/rs.3.rs-3094340/v1

Additional Declarations: There is **NO** Competing Interest.

Nutrient subsidies restructure coral reef dissolved carbon fluxes via biogeochemical cascades

Nyssa J Silbiger[1], Megan J. Donahue[2], Benjamin Hagedorn[3], Danielle M. Barnas[1], Hendrikje Jorissen[2,4], Jamie R. Kerlin[1], Rayna McClintock[4], Emily Nixon[5], Wesley J. Sparagon[4], Maya Zeff[1], Craig E. Nelson[4]

[1] Department of Biology, California State University, Northridge, CA, USA

[2] Hawai'i Institute of Marine Biology, University of Hawai'i at Mānoa, Kāne'ohe, Hawai'i , USA

[3] Department of Geological Sciences, California State University, Long Beach, CA, USA

[4] Daniel K. Inouye Center for Microbial Oceanography: Research and Education, Department of Oceanography and Sea Grant College Program, University of Hawai'i at Mānoa, Honolulu, Hawai'i , USA

[5] Scripps Institution of Oceanography, University of California, San Diego, CA, USA

Email: nyssa.silbiger@csun.edu

Author Contributions: All authors collected data, edited the manuscript, and gave final approval. NJS, MJD, CEN conceptualized the design. NJS analyzed the data and wrote the manuscript.

Competing Interest Statement: We do not declare any competing interests.

Classification: Biological Sciences - Ecology; Environmental Sciences

Keywords: Submarine groundwater discharge, ecosystem metabolism, biogeochemical cascade, allochthonous inputs

This PDF file includes:

Main Text
Figures 1 to 5
Tables 1 to 2
Methods

Abstract (139/150 words)

Marine organisms are increasingly recognized as both responding to and driving biogeochemical changes in their environment. The addition of exogenous resources to the ocean, such as nutrients, that alter organismal physiology can lead to biogeochemical cascades wherein these solutes both alter water chemistry directly and indirectly by changing biological processes that influence water chemistry. To quantify how allochthonous nutrients drive biogeochemical cascades, we measured a suite of biogeochemical parameters during synoptic spatial surveys across two reefs in Mo'orea, French Polynesia conducted day and night at both low and high tide in two different seasons. These data were used to build a model that demonstrates how inputs of nutrients to coral reefs via submarine groundwater discharge directly alter reef metabolism with cascading effects on the cycling of dissolved organic and inorganic carbon that regulate productivity, calcification, and the microbial loop.

Main Text

Introduction

Exogenous sources of nutrients and energy, or allochthonous inputs, to marine ecosystems can have cascading impacts on ecosystem functioning [1,2]. For example, nutrients upwelled from the deep ocean into the coastal zone promote the growth of kelp, foundational species that provide habitat and food for a diverse kelp forest community [3]; similarly, freshwater inputs from glaciers create thriving arctic ecosystems by facilitating sea ice algae, which ultimately support 70% of polar bear diets [4]. Shallow, nearshore ecosystems, like many coral reefs, are particularly affected by allochthonous inputs of nutrients and other solutes, which are commonly transported by freshwater connections from land to sea [5,6]. Natural allochthonous inputs can be beneficial to coral reefs: nutrients from seabird guano can elevate critical ecosystem functions, like herbivory, by 3.2 times relative to sites where seabird populations are diminished [7]. In contrast, anthropogenic allochthonous inputs (e.g., urban and agricultural run-off and sewage effluent) can negatively alter competitive dynamics on reefs leading to macroalgal blooms, coral disease, and shifts in community structure [8–10]. Despite the known effects of allochthonous inputs on food-web dynamics and community stability in marine ecosystems, the mechanisms of action and interaction of biotic and abiotic processes leading to ecosystem consequences remain unclear. As climate change, coastal development, and other anthropogenic stressors continue to alter both natural and anthropogenic allochthonous inputs to the ocean, it is critical to understand both the direct geochemical and biologically mediated effects of these inputs on coastal ecosystem functioning.

Biological and geochemical processes continuously interact, altering the concentration of dissolved solutes that ultimately regulate ecosystem metabolism. For example, recent studies have highlighted the importance of primary producers in the dynamics of dissolved CO_2 concentrations and subsequent pH variability in coastal ecosystems [11–13]; in turn, pH variability

affects other biological processes like net ecosystem calcification (NEC) [11,14,15]. Allochthonous inputs, such as added nutrients, can magnify this biogeochemical interaction: a coral reef study showed that a chronic low-level increase in inorganic N and P elevated pH variability nearly thirty-fold by enhancing net ecosystem production (NEP) [16]. There has been a growing acknowledgement that organisms not only respond to their geochemical environment, but simultaneously modify it: in coral reefs and other highly productive coastal ecosystems, there has been a particular focus on the inorganic carbon feedback loop (NEP → pH → NEC) [11,14,16–19]. However, changes to ecosystem metabolism can also alter the composition and quantity of the organic carbon pool [20–22]. For example, field and lab studies both show that benthic community composition directly alters the composition of dissolved organic matter (DOM) [20,21]. Added nutrients can also indirectly alter the relationship between metabolism and DOM composition, likely through augmented productivity [21,23]: in one study, corals responded to a 3-fold increase in N with a ~40% and ~150% increase in humic and proteinaceous DOM, respectively [21].

While these studies highlight that the biological response to allochthonous nutrients can affect the inorganic or organic carbon pools, few studies explicitly link organic and inorganic biogeochemistry. Here, we advance the field by demonstrating that allochthonous inputs create “biogeochemical cascades", whereby the addition of new nutrients to a system indirectly affects both dissolved organic and inorganic carbon pools by changing the patterns of uptake and release of carbon by benthic organisms (Fig. 1). Understanding how allochthonous inputs can drive interactions between biological and geochemical processes is applicable to all ecosystems, but especially to coral reefs where terrestrial nutrient sources alter local biogeochemistry, drive phase shifts between coral and macroalgae [24], and, ultimately, affect ecosystem metabolism.

Submarine groundwater discharge (SGD) is a natural land-sea connection that is found worldwide [25,26] and is a template to explore how allochthonous inputs affect interactions between biological and geochemical processes. SGD has a complex mixture of components and is a major source of new solutes that can influence coastal salinity, carbonate dynamics, nutrient fluxes, and the composition and concentration of dissolved organic matter [27–29]. SGD-driven solutes have been linked to changes in algal species richness [30,31], coral and macroalgal growth [32,33], bioerosion [32,34], and net ecosystem production and calcification [15,35] on coral reefs. The flux of SGD and its unique biogeochemical composition vary tidally, seasonally, and spatially, and are affected by both natural and anthropogenic processes such as precipitation, coastal development, freshwater harvesting, and wastewater handling [36,37]. Differences in the chemical composition of SGD can also have differential impacts on local biology. For example, in locations where total alkalinity (TA) in SGD is higher than the receiving waters [28], SGD may buffer corals from low pH [28,38,39], while locations where TA in SGD is lower than the receiving waters may compound the effects of low pH on calcifiers. Climate change and increasing coastal population densities will alter the flux and composition of SGD [40,41] and our ability to protect coastal ecosystem services is directly impacted by our understanding of how SGD affects biological and geochemical processes.

We consider the hypothesis that allochthonous inputs from SGD create biogeochemical cascades; i.e., that elevated nutrients affect the production and feedbacks between organic and

inorganic carbon (Fig. 1). We test our hypothesis by resolving spatial gradients of reef metabolism and biogeochemistry across diel, tidal, and seasonal timescales at two shallow coral reef sites with differing coastal environmental conditions in Mo'orea, French Polynesia (Fig. 2). Using structural equation models in a Bayesian framework, we characterized the direct geochemical and indirect biologically mediated effects of SGD on the concentration and composition of dissolved organic and inorganic carbon pools. We have four main conclusions. First, we show that the differences in the composition of SGD (i.e., salinity, nutrients, fDOM, pH, and TA) – likely a result of contrasting hydrogeology and local human population density – create different relationships between geochemical and biological processes, especially the dynamics of inorganic carbon. Second, our data demonstrate that SGD creates biogeochemical cascades that have downstream effects on net ecosystem metabolism, specifically production, calcification, and the transformation of dissolved organic matter. Third, we show that SGD mediates interactions between multiple ecosystem functions: when biologically driven processes, like NEP, are elevated it can either dampen or augment the direct effect of SGD on local biogeochemistry. Lastly, we show that differences in reef "template", such as flow conditions, coastal geology, and benthic community composition altered the pathways within the biogeochemical cascade. Our results emphasize that SGD has a substantial effect on coastal biogeochemistry and ecosystem functioning and will facilitate future work to better understand the role of allochthonous inputs on biogeochemical cascades.

Results and Discussion

Fundamental differences in groundwater discharge chemistry in adjacent aquifers

At two fringing coral reef sites in Mo'orea, French Polynesia (Fig. 2a) with markedly different flow conditions (Fig. 2f), we synoptically sampled water from 20 points arrayed across a 15000 - 27000 m^2 area (Fig 2b, c). Each array was sampled eight times (both high and low tide each day and night; Fig. 2d) in both wet and dry seasons (August 2021 and March 2022), supplemented with high resolution time series sampling at each groundwater seep. SGD delivered significant quantities of freshwater, up to 9.34 ± 4.03 and 7.20 ± 3.18 cm d^{-1} at Varari and Cabral, respectively. At both sites, SGD had elevated nutrient concentrations relative to ambient seawater, including nitrate plus nitrate (N+N), ammonium (NH_4^+), silicate (SiO_3^{2-}), and phosphate (PO_4^{3-})(Fig. 2e); therefore delivering large fluxes of inorganic nutrients to the nearby reef. Nutrients are expected to be higher in SGD relative to oligotrophic seawater, such as coral reefs, due to higher concentrations of nitrogen in rainwater (~ 1 µmol L^{-1} N+N in Mo'orea [42]), downward leaching of N and P from terrestrial matter and/or dissolution of seabird guano [43–45], and high SiO_3^{2-} and PO_4^{3-} values from mineral weathering [46,47]. Natural SGD is an important source of new nutrients to coral reefs [25,29] and can benefit native algae and corals [32,48]. However, the highly elevated values at our sites (e.g., up to ~ 280 µmol L^{-1} of N+N at Varari; Table 1) may be a result of septic drainage, fertilizer from nearby agriculture, and other anthropogenic activities contaminating the groundwater [42]. The SGD was also a significant source of humic-derived fDOM at both sites, and a significant source of proteinaceous fDOM at Cabral during the dry season. Prior studies have also found elevated concentrations of fDOM in SGD and have suggested that quantity and composition of fDOM is a good geochemical tracer for SGD [27]. The added fDOM to the reef, if labile, could fuel the microbial loop [49] and augment ecosystem metabolism [50].

The inorganic carbon pool, however, was particularly different between the sites: at Cabral, total alkalinity (TA) was highly depleted relative to ambient seawater, while at Varari it was highly elevated

(Fig. 2e; Table 1). This pattern of contrasting TA values in the SGD of nearby sites has also been shown in other high volcanic islands of similar geologic age, like O'ahu, Hawai'i [15,27] and is likely a result of the fresh groundwater passing through different aquifers, with different proportions of more soluble carbonate vs. less soluble silicate minerals. These different TA values between the two sites could either compound (Cabral) or buffer (Varari) the negative effects of the low pH groundwater on calcification [38], which had pH values reaching as low as ~7.2 in the SGD at both sites (Table 1).

Tidal patterns indicate a direct influence of SGD on reef biogeochemistry

The degree to which the low tide chemical composition of each site reflected the SGD composition was strikingly different between the two sites. At Varari, a site with faster, unidirectional (alongshore) water flow (Fig. 2f), there was a clear separation between tidal cycles, indicating a strong direct influence of SGD on reef biogeochemistry, with low tide having higher nutrients, humic fDOM, and SiO_3^{2-} as well as lower salinity relative to high tide (Fig 3a,c). At Cabral, a site with slower, tidally-dependent, cross-shore flow, there were also differences in the biogeochemistry across tidal cycles, but with less distinction between tides (Fig. 3b,d). While Cabral exhibited lower salinity, higher SiO_3^{2-}, and lower TA during low tides, as expected from the composition of SGD at Cabral (Table 1), the N+N and PO_4^{3-} concentrations did not vary tidally across the reef, even though both of these solutes were highly elevated in the SGD. Given the longer water residence time at Cabral, it is likely that there was more time for the reef organisms to utilize the nutrients, decoupling the nutrient concentrations from other SGD solutes and masking the expected tidal effect of nutrients.

Diel patterns in reef biogeochemistry indicate an indirect effect of SGD via biological processing

The clear difference in the biogeochemistry across diel cycles indicated strong biological control of the seawater chemistry, with important differences between the two sites (Fig. 3). At Varari, where SGD delivers relatively high TA, daylight hours (afternoon and dusk) had a higher pH, lower TA, and lower proteinaceous fDOM relative to dark hours (midnight and dawn). The diel pH patterns align with expected decreasing water column CO_2 from daytime net photosynthesis and increasing CO_2 from nighttime respiration. The diel patterns in TA also indicate that the biological control of TA from calcification outweighed the geochemical controls of high alkalinity SGD flowing onto the reef during low tide: when organisms calcify, TA is removed from the water column; during dissolution, TA is released into the water column [51,52]. This contrasts with results from Cabral, where pH and TA were orthogonal to each other on the reef: pH was correlated with diel patterns while TA was correlated with tide (Fig. 3). That is, pH was biologically controlled, while TA remained geochemically controlled. Dawn low tides had the most distinct biogeochemistry at both sites, with the highest concentrations of fDOM and the lowest pH. As expected, these sunrise samples had the lowest pH after a night of respiration compounded by the low tide flux of low pH SGD onto the reef. The elevated fDOM may correspond to a rapid increase in coral and algal exudates with the onset of photosynthesis at sunrise, combined with elevated fDOM from the low tide flux of SGD onto the reef.

Allochthonous nutrient inputs drive biogeochemical cascades

To illustrate how allochthonous nutrient inputs drive biogeochemical cascades in these reef ecosystems, we used Bayesian Structural Equation Models (SEM) to explore how diel, tidal, and spatial patterns in SGD related to biological responses and geochemical feedbacks (Fig. 4). In general, our model revealed that SGD-derived nutrients augmented both net production and microbial respiration, that the indirect effect of SGD on NEP changed both the local pH conditions and humic-like fDOM concentrations in the water column, that the altered pH of the seawater then modified NEC rates, and that the altered NEC rates then led to changes in the concentration of proteinaceous fDOM. Further, the

213 relationships between each of the measured variables in the model were generally consistent between
214 seasons, but there were distinct differences between sites due to unique reef templates (Fig. 5). In
215 particular, differences in flow conditions and the geochemical makeup of the SGD mediated the indirect
216 relationships between SGD and ecosystem metabolism by modifying biological uptake/production rates of
217 dissolved solutes and by changing the pH buffering capacity of seawater which can affect calcification
218 rates. Below we describe the statistical outcomes for each of the six equations in the SEM model (Table
219 2).
220
221 ***SGD is a significant source of allochthonous nutrients to coral reefs***
222 The SEM captures the expected relationships between SGD and nutrient concentrations as
223 described above. Specifically, there was a strong positive relationship between SiO_3^{2-} (a proxy for SGD)
224 and N+N (Fig. 5a,l; Fig. S1-S2) at the higher flow site (Varari), while N+N concentrations were unrelated
225 to SiO_3^{2-} at the lower flow site (Cabral) (Fig. 5a,l; Fig. S3-S4). This decoupling of SGD and N+N at the site
226 with much longer residence times (Cabral) may indicate greater biological uptake of SGD-sourced N+N
227 across sampling stations; in contrast, the faster-moving water at Varari (Fig 2) and higher concentrations
228 of N+N at seep (Table 1) allowed the coupling of SGD and N+N to be maintained across sampling
229 stations. Importantly, nutrients measured from seawater over the reef are "leftovers" after biological
230 modification and do not necessarily indicate the total amount of nutrient delivery [20].
231
232 ***Allochthonous nutrient inputs drive increased ecosystem productivity and respiration***
233 SGD generally increased net ecosystem production potential (NEP) during the day, but this
234 relationship was dependent on temperature and seasonality. Specifically, elevated N+N from SGD at the
235 high flow site (Varari) increased NEP during the dry season but not the wet season (Fig. 5f,m; Fig. S1-
236 S2). At the low flow site (Cabral), there was a slight positive relationship between NEP and N+N during
237 the wet season, although neither times were statistically significant (Fig. 5f,m; Fig. S3-S4). The weaker
238 relationship between NEP and N+N at Cabral may reflect that nutrient drawdown decouples SGD from
239 nutrient concentration more strongly where flow rates are slower. Further, the differences in the total
240 standing stock of producers may lead to different equilibriums for nutrient uptake, which would also drive
241 differences between NEP and N+N between the sites. At night, N+N generally increased microbial
242 respiration, which means biological responses from the SGD could further acidify the already low pH reef
243 water at night (Fig. 5f,m; Fig. S1-S2). Temperature was the strongest predictor of NEP at both sites in this
244 study (Fig. 5m,g; Fig. S1-S4), with significant positive relationships between temperature and NEP during
245 both seasons at Varari and during the dry season at Cabral. Temperature is often a strong driver of NEP
246 on coral reefs [53], and temperature increases in response to solar radiation on shallow reefs and may
247 decrease with SGD, which can cool coastal water [54].
248
249 ***Indirect effects of SGD on pH mediated by ecosystem metabolic responses***
250 Our data demonstrated how SGD can amplify diel pH dynamics on coral reefs by increasing
251 productivity during the day and respiration at night. SGD-enhanced NEP rates drove substantial changes
252 in pH, with significant positive relationships between NEP and pH at both sites and during both seasons
253 (Fig. 5c,n; Fig. S1 - S4). Additionally, the biological effect of NEP on pH either completely masked or
254 modified the expected negative relationship between SGD and pH (Fig. 5c,n; Fig. S1 - S4). During the dry
255 season, augmented nutrients that generally elevated net photosynthesis and microbial respiration are
256 increasing pH during the day and decreasing pH at night, regardless of the addition of low pH waters from
257 SGD. This pattern has also been shown in Hawai'i [15] and the Great Barrier Reef [55], where reefs
258 experience greater biological than geochemical controls of pH at sites with SGD [55]. During the wet
259 season, when there was a significant interaction between NEP and SGD on pH at both sites, the negative

effect of SGD on pH was present, but was altered by changing NEP (Fig. 5c,n; Fig. S2, S4). Further, at night when the reef was net respiring, SGD amplified the already low pH waters and decreased pH even more than expected from biology alone. These low pH conditions during nighttime low tides could decrease net calcification and potentially drive reefs into net dissolution, especially at locations where the TA in the SGD is depleted.

Cascading impacts of SGD on community calcification via metabolic controls on carbon flux

The altered pH environment, resulting from both the direct (from freshwater) and indirect effect (from altered NEP) of SGD, further impacted ecosystem function by changing net ecosystem calcification potential (NEC) (Fig. 5h,i,o; Fig. S1-S4). However, the relationship between pH and NEC differed between the high and low alkalinity sites. At Varari, the high alkalinity site, there was a positive relationship between pH and NEC as is typically expected on coral reefs [52], although the relationship was not statistically significant during the wet season (Fig. 5h,o; Fig. S1-S2). Prior studies have found elevated TA in SGD [15,28] and it has been hypothesized that this elevated TA may help buffer coral reefs from low pH waters in the SGD and possibly even from ocean acidification [28,38,39]. Conversely, at the low alkalinity site (Cabral), there was no relationship between pH and NEC (Fig. 5h,o; Fig. S3-S4), potentially due to depleted TA in the SGD source water making it more difficult for corals to calcify. Differences in benthic coral composition and total cover may have also affected the differences in the relationship between pH and NEC between the sites. An alternative hypothesis is that the higher concentrations of nutrients over the reef at this site, average N+N concentration at Cabral is 0.17 μmol L^{-1} higher than Varari, altered the expected relationship between NEC and pH. A prior laboratory study showed a similar decoupling between aragonite saturation state and NEC with increasing nutrient concentrations [16]. Temperature also increased NEC and was the dominant driver of NEC in our study (Fig. 5i,o EM;Fig. S1-S4). Temperature is often an important driver of NEC on coral reefs [56–58]. These data demonstrate that differences in the components of the SGD, especially the concentration of TA, could have significant downstream impacts on coral reef ecosystem functioning.

Whole ecosystem biogeochemical cascades translate groundwater inputs into DOM production

Finally, our data showed both direct and biologically mediated effects of SGD on the composition of dissolved organic matter fluxes. SGD was associated with the direct enrichment of both humic and proteinaceous fDOM at both sites, although the effect size between SGD and both fDOM components were nearly twice as high at Cabral (Fig. 5d,k,p,q; Fig. S1-S4). Differences in the age of the aquifers or the microbial activity in the SGD could be responsible for differences in the SGD-derived fDOM between the two sites [27,59]. Beyond the direct delivery of fDOM, NEP increased humics during the day and decreased humics at night (Fig. 5e,p; Fig. S1 - S4), likely because producers release exudates during the day and microbial respiration utilizes DOM at night [60]. NEC generally decreased proteinaceous fDOM in the water column (Fig. 5j,q; Fig. S1-S4), which is opposite of what we expected based on studies showing corals releasing significant amounts of proteinaceous fDOM [20,21]. However, prior studies showing these relationships were in closed systems (either aquarium or reef tent) that were dominated by corals. The sites in the current study had < 20% coral cover and it is likely that consumption of fDOM by microbial respiration outpaced the production by corals. Nevertheless, the interactions between the biological and geochemical controls of the organic carbon pool clearly indicate that SGD could fuel the microbial loop both through the direct addition of DOM and indirectly through biological changes as a result of the SGD. Additionally, as climate and land-use continues to change it will alter the concentration and composition of DOM in groundwater [59], which could further impact ecosystem functioning on coral reefs.

Importance of understanding biogeochemical cascades in coastal ecosystems

Overall, our data support the premise that allochthonous nutrient inputs can stimulate biogeochemical cascades, but the patterns between the geochemical and biological components are dependent on the "template" of the site (e.g., flow rates, benthic community composition, quality of the SGD, human influence, etc). While understanding the effects of SGD on coastal processes is important because of its worldwide distribution [25,26,61], SGD is not the only factor that can spark biogeochemical cascades. For example, loss of dominant species, or phase shifts, can indirectly affect multiple ecosystem processes as mediated by changes in biogeochemistry [14,62], and phase shifts are becoming increasingly common on coral reefs as a result of anthropogenic disturbances [63]. Changes to rivers and streams from deforestation, pollution, or changing precipitation can also add new solutes and increase sedimentation [64] that could create biogeochemical cascades, leading to downstream impacts on ecosystem functioning and ecosystem services. Using a biogeochemical cascade approach allows us to uncover both the direct and indirect drivers of ecosystem processes, reinvigorating classical frameworks in ecology that connect ecosystem ecology to humans and society [65].

Figures and Tables

Table 1. SGD endmembers from dug beach pits and inland springs for each measured parameter in the study. Missing data are indicated with a dash.

Parameter	Unit	Cabral Beach Pit	Cabral Spring	Varari Beach Pit 1	Varari Beach Pit 2
Salinity	psu	3.11	0.44	2.89	9.67
Total Alkalinity	$\mu mol\ kg^{-1}$	1959.29	1335.71	3813.31	5389.84
pH_T	$\mu mol\ L^{-1}$	7.65	7.24	7.18	7.73
Ammonium (NH_4^+)	$\mu mol\ L^{-1}$	5.41	0.89	1.6	0.79
Nitrate + Nitrite (NO_x)	$\mu mol\ L^{-1}$	32.5	19.77	32.63	279.15
Phosphate (PO_4^{3-})	$\mu mol\ L^{-1}$	1.85	4.06	2.6	1.57
Silicate (SiO_3^{2-})	$\mu mol\ L^{-1}$	650.73	737.49	713.06	229.28
Humic fDOM	Raman Units	0.08	0.08	0.12	-
Proteinaceous fDOM	Raman Units	0.06	0.12	0.06	-
Temperature	°C	-	30.18	29.06	-

Table 2. Model formulas and justification for each equation within the structural equation models (Fig. 4).

Equation within SEM	Model formula	Justification
1	**N+N ~ SiO_3^{2-}**	Equation 1 is based on our understanding that N+N is positively associated with SGD [15,25,27,29]. Here, we use SiO_3^{2-} as a proxy for SGD [66]. Notably, SiO_3^{2-} and salinity were highly correlated on the reef (Fig. 2e). However, the range in SiO_3^{2-} was an order of magnitude higher on the reef than salinity allowing for a higher signal to noise ratio.
2	**NEP ~ (Day or Night × N+N)**	We hypothesized that NEP increases with temperature and that the relationship between NEP and N+N is dependent on whether it is dark (N+N increases microbial respiration) or light (N+N increases photosynthesis).
3	**pH ~ NEP × SiO_3^{2-}**	Equation 3 is based on our understanding that SGD has a low pH [67] and that there is a positive relationship between NEP and pH on coral reefs [15]. We also hypothesized that the ability to detect the relationship between pH and SGD could be dampened or augmented by NEP.
4	**NEC ~ pH + Temperature**	Equation 4 is based on the knowledge that NEC is affected by both pH and temperature [52]
5	**Humic fDOM ~ (Day or Night × NEP) + SiO_3^{2-}**	In equation 5, we hypothesize that humic fDOM is elevated in SGD [27], and also that humic fDOM increases when macrophytes are photosynthesizing and decreases as it is consumed during microbial respiration [21,22].
6	**Proteinaceous fDOM ~ NEC + SiO_3^{2-}**	For equation 6, we hypothesize that proteinaceous fDOM is elevated in SGD [27], and also that it is affected by the presence of corals [21] and, therefore, NEC.

Figures and figure legends

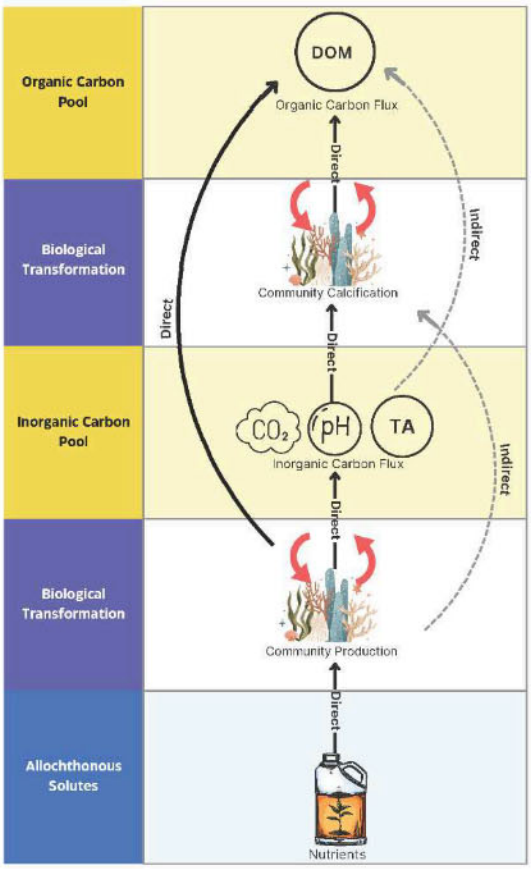

Figure 1: Conceptual diagram of a biogeochemical cascade on coral reefs. Added solutes to an ecosystem can create biogeochemical cascades where geochemical parameters indirectly influence each other by altering biological processes, and biological parameters indirectly influence each other by altering geochemical processes. Solid arrows indicate direct relationships and dashed arrows indicate indirect relationships.

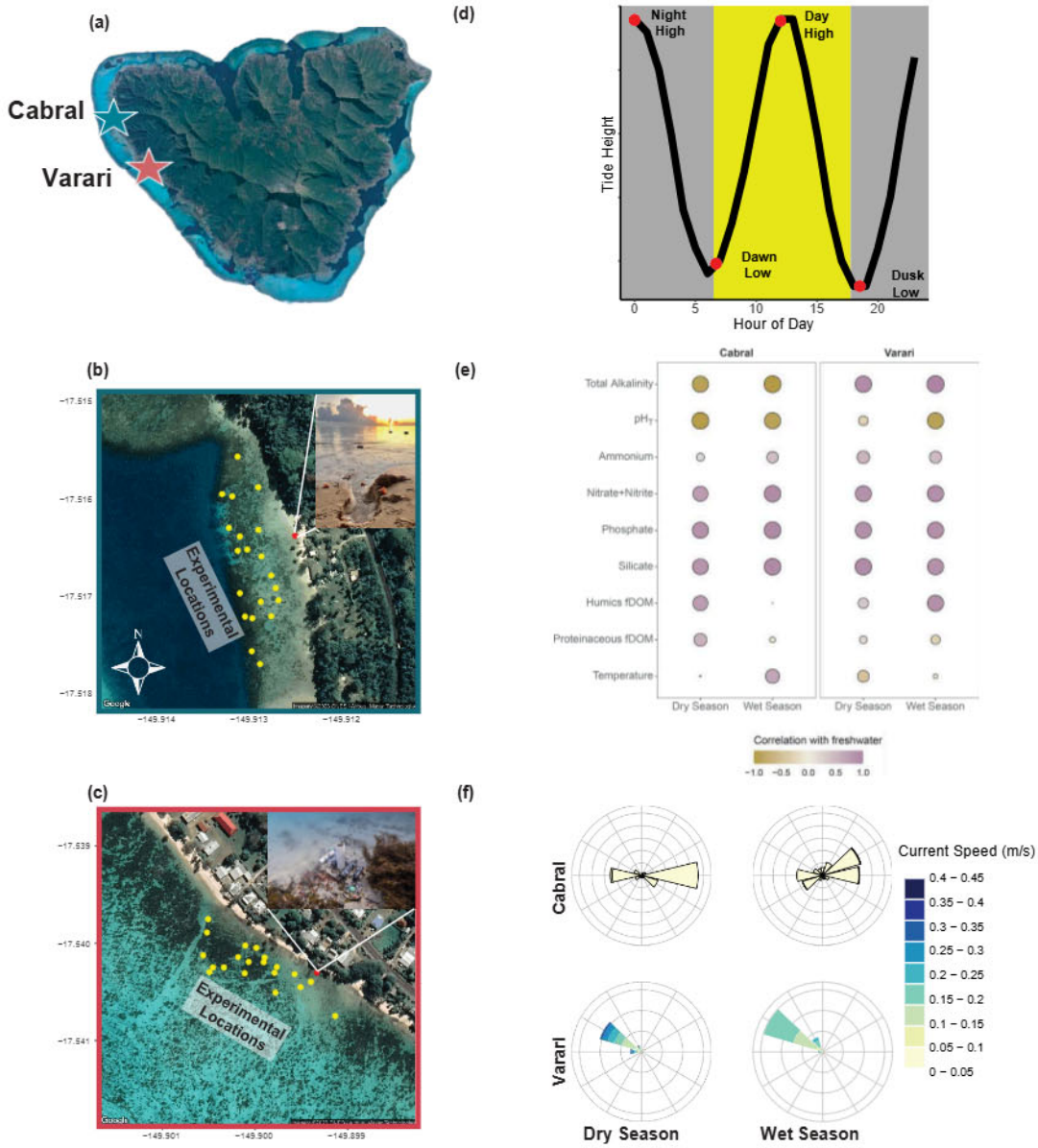

Figure 2: (a) A map of Mo'orea, French Polynesia with stars indicating the two field sites (Cabral in green and Varari in red). Insets on the left show maps of Cabral **(b)** and Varari **(c)**, with the experimental locations in yellow and the selected SGD seepage point in red. A picture of each seepage point is located in the top right corner of the maps. Inset **(d)** shows the general sampling design for water collection for the 21 coincident samples. As Mo'orea is an amphidromic point, high tide and low tide are at the same general time all year round. Inset **(e)** illustrates the correlation of each measured parameter with freshwater where positive relationships with freshwater are indicated in purple and negative relationships with freshwater are indicated in yellow. The size of the circle is related to the strength of the correlation, with bigger circles having stronger correlations. **(f)** A windrose plot of current speed (visualized with color) and direction for each site and season. The dry and wet season collections were in August and March, respectively.

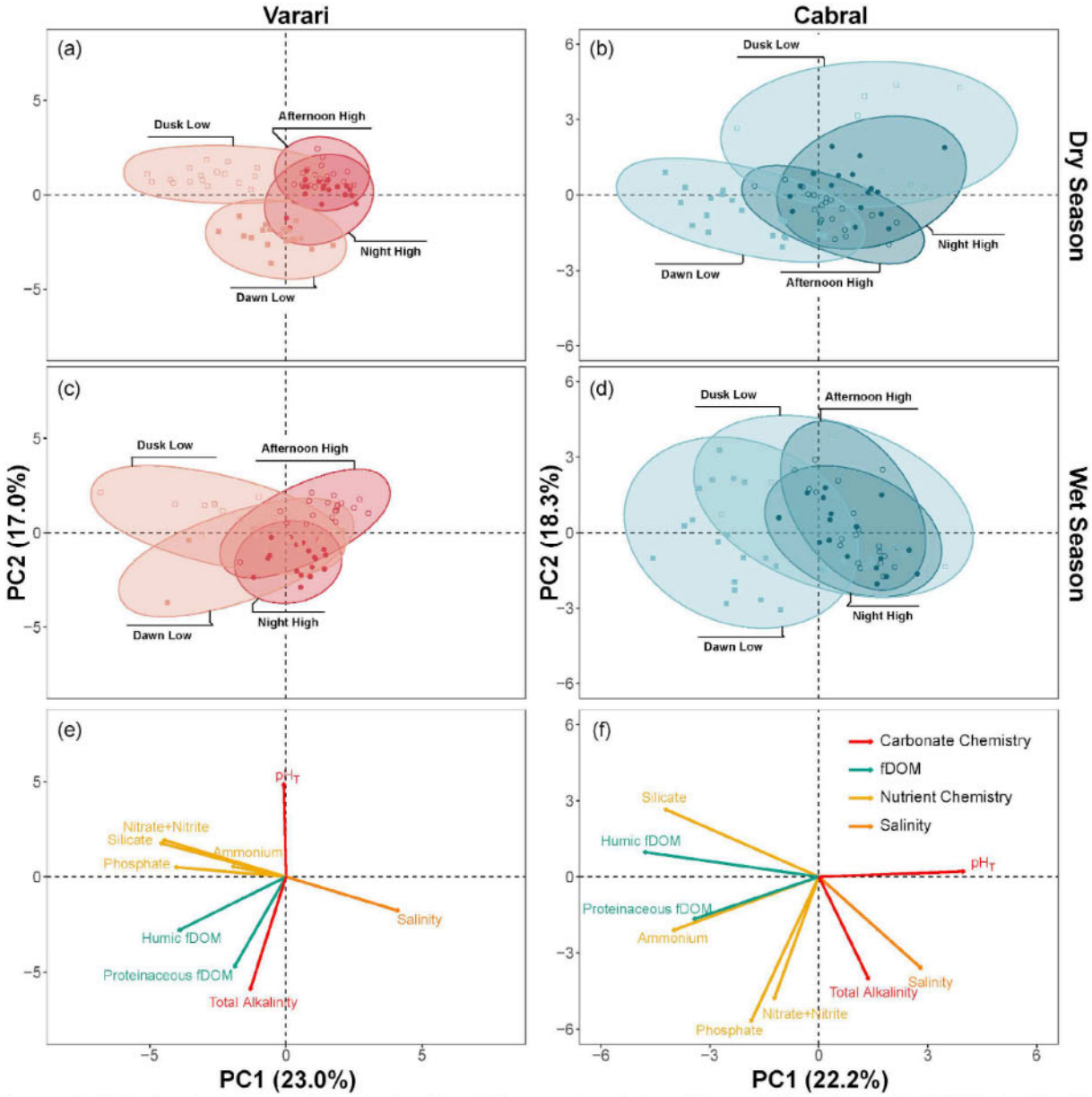

Figure 3: Principal component analysis of reef biogeochemistry at **(a,c,e)** Varari and **(b,d,f)** Cabral for the **(a,b)** dry season and **(c, d)** wet season. Each point represents a single water sample at a single experimental location, with open circles representing daylight (afternoon and dusk) and closed circles representing dark hours (midnight and dawn). The dark shaded polygons represent high tide and the light shaded polygons represent low tide. Points closer together have more similar biogeochemistry than points further apart. Insets (e) and (f) show the biplots for each site, where the length of the arrow represents the relative strength of the loading.

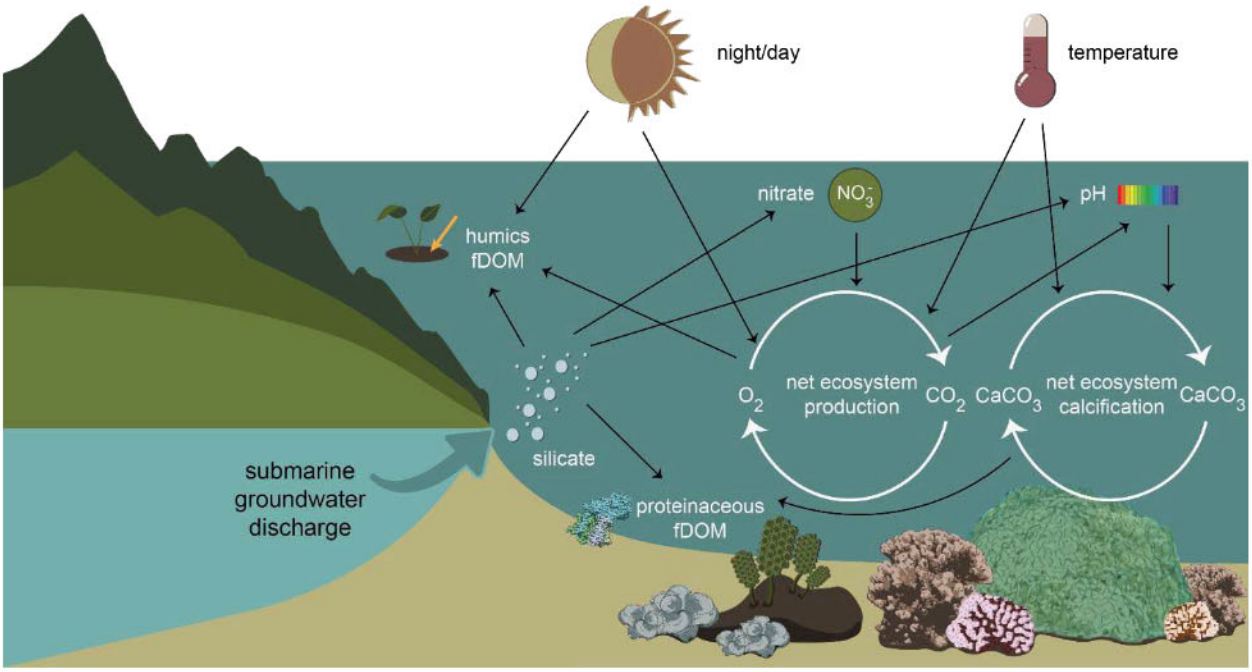

Figure 4: Visualization of the structure equation model (SEM). Black arrows indicate direct relationships included in the SEM. Table 2 shows the model formulas and the justification for each model within the SEM.

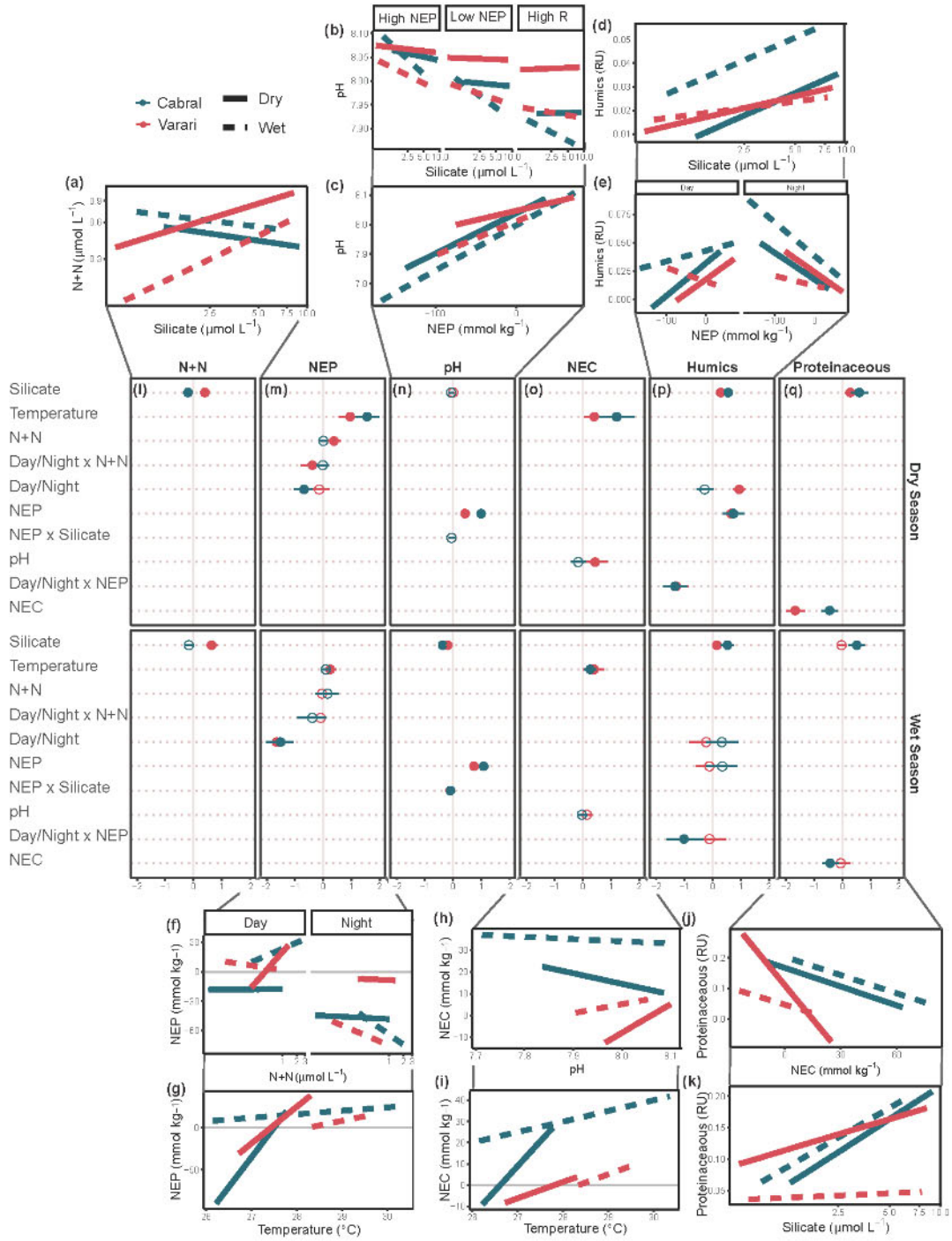

Figure 5: Results from the structural equation model. The central plots **(l - q)** show the effect size and 95% BCI for all parameters included in each equation. Labels on the top of each effect size plot are the dependent variables, and the top boxes are results from the dry season and the bottom boxes are from the wet season. Lines that do not overlap zero are considered statistically significant effects. The call outs **(a-e, f-k)** visualize the best fit lines for each model, with raw data shown in Supplemental Figures S1 - S4. Solid lines are from the dry season and dashed lines are from the wet season. Cabral is shown in green and Varari is shown in red.

Materials and Methods

Site descriptions

Our study was conducted at two sites on the western side of Mo'orea, French Polynesia (Fig. 2a-c), a high volcanic tropical island with microtidal conditions. The two experimental sites were chosen based on discussions with local residents who had historical knowledge of SGD seepage points around Mo'orea, followed by preliminary radon and salinity surveys. To ensure that SGD was the dominant source of freshwater and land-based solutes to the coastline at the experimental sites, we selected locations that were at least 0.7 km away from any rivers or streams.

The northernmost site, Cabral (Fig. 2b; -17.52° S and -149.91° W), is much less populated, with a single family living along most of the coastline. The reef at Cabral has 20% coral cover, dominated by *Porites* spp. and *Pavona* sp., with 58% macroalgal cover. The flow direction at Cabral is tidally driven and the flow speed is highly dampened relative to Varari (0.018 ± 0.00023 m/s [mean ± SE]; Fig. 2f). Cabral has several seepage points spread out along the coastline, with likely additional ones further on the reef (pers comm T. Cabral). There are at least two known inland springs at Cabral where we were able to sample the source water with permission, although we are unable to share the locations of the springs to protect the water rights of the local community.

The southernmost site, Varari (Fig. 2c; -17.54° S and -149.90° W), is a relatively populated area with several vacation rentals and local residents living along the coastline. Varari has approximately 13% coral cover, dominated by *Porites rus, Pocillopora acuta,* and *Montipora* spp., and 58% macroalgal cover. The site has a consistent northwesterly unidirectional flow, with the fastest flow speeds when water levels are high (0.15 ± 0.00092 m/s [mean ± SE]; Fig. 2f). The SGD seepage points are clustered in one area and always subtidal and conspicuous, with freshwater water bubbling up through the sand near the shoreline. The location of the inland spring(s) that feeds these SGD seeps are currently unknown and there are no local accessible wells.

Experimental set-up

We characterized the biogeochemistry and benthic community composition at 20 experimental locations plus one seepage point at each site (Figs. 2b-c). Benthic community composition was assessed in a 1 m^2 area around each experimental location using the quadrat point count method from 100 evenly spaced cross hairs. For the 20 reef locations, we collected discrete water samples directly from the benthos across tidal (high/low), diel (day/night), and seasonal (dry/wet season) timepoints for a total of eight measurements per location (n = 320 water samples total). The depths of the reef sampling locations were all less than 1.3 m from the surface. At the selected seepage points for each site, we collected additional samples to better characterize the composition of the incoming groundwater (n = 25 at Varari and n = 24 at Cabral). We also collected water samples at the reef crest ~ 1km from each site (n = 13 for Varari and n = 7 for Cabral) to characterize the incoming ambient seawater conditions. To determine groundwater endmembers, we sampled an inland spring and a beach pit at Cabral and two beach pits at Varari (Table 1). Sampling occurred in August 2021 and March 2022 in the dry and wet seasons, respectively.

Water samples for nutrients (N+N, NH_4^+, SiO_3^{2-}, PO_4^{3-}), fluorescent dissolved organic matter (fDOM), total alkalinity (TA), pH, and salinity were collected either by hand with an acid washed HDPE bottle or using a subsurface automated sampler (SAS) [68]. Nutrient and fDOM samples were filtered with a 0.22 µm Sterevix either *in situ* before entering an acid washed Mylar bag on the SAS or immediately after collection with a syringe. Nutrients were frozen (-20°C) and stored in 50 ml falcon tubes and fDOM samples were refrigerated (4°C) and stored in amber glass bottles. To measure TA, seawater was pumped into a Tedlar bag that was pre-fixed with 50% saturated $HgCl_2$ in deionized water or immediately

fixed after collection—all TA samples were stored in amber HDPE bottles in a cool dark location prior to processing. TA samples collected directly from springs or from low salinity seawater (psu <20) were collected in duplicate, where one sample was fixed as described above and a second sample was filtered and refrigerated, as suggested by Mos et al. [69]. However, the differences between the two samples were minor (< 5 µmol kg^{-1}); therefore, the fixed samples were used in all statistical analyses for consistency. pH and salinity were measured immediately after collection. pH was measured on the total scale with a Tris calibrated glass electrode (Thermo Scientific Orion ROSS Ultra pH/ATC Triode) paired with a Thermo Scientific trace digital thermometer (5-077-8, accuracy = 0.05 °C, resolution = 0.001 °C; Control Company, Friendswood, TX, USA) following Dickson SOP 6a [70]. *In situ* temperature was measured with Onset Conductivity Temperature loggers (U24-002-C, accuracy = 0.1 °C, resolution = 0.01 °C, Bourne, MA, USA) and *in situ* pH was back-calculated using the seacarb R package [71]. Salinity was measured immediately after collection using a DuraProbe 4-cell conductivity electrode on an Orion Star multimeter. All water sample storage/measurement vials were acid washed and thrice rinsed with sample water.

Sample processing for nutrients, fDOM, and total alkalinity

Nutrients (N+N, NH_4^+, SiO_3^{2-}, PO_4^{3-}) were analyzed on a Seal Analytical AA3 nutrient autoanalyzer at the SOEST laboratory for analytical biogeochemistry (reported error [coefficient of variance]: 0.5% for SiO_3^{2-}, 0.3% for N+N, 0.2% for PO_4^{3-}, 1.3% for NH_4^+). Characterization of fDOM on 0.22 µm filtrate stored for no more than 2 months at 4℃ was done on an Horiba Aqualog 3-D scanning fluorometer according to [27]. fDOM was then grouped into "Humics" (visible + marine-like humics) and "Proteinaceous" (tryptophan-like + tyrosine-like) for analysis based on descriptions by Coble [72]. Total alkalinity samples were analyzed on a T-5 Mettler-Toledo automatic titrator for Dickson SOP 3b [70]. The accuracy (better than 5 µmol kg^{-1}) of the titrator was tested against a certified reference material from the Dickson lab every day.

Radon measurements and SGD calculations

In addition to biogeochemistry sampling, we also measured radon near each seepage point for ~24 hours to calculate SGD fluxes. Dissolved radon activities (5-minute timestep) were measured by the Durridge RAD-7/Rad Aqua monitor, connected to a Rule 1100 GPH bilge pump that ran over multiple tidal cycles. The pump inlet was always located about 10 cm above the seafloor, to avoid clogging with sediments. Wind speed data (30-minute timestep) for atmospheric radon loss computations were collected at Hotel Les Tipaniers, about 2.5 - 3 km north of our study area. Radon and conductivity/temperature were also measured in groundwater sampled at the Cabral Spring (located ~100 m inland from the Cabral monitoring site) and from 6 water supply wells distributed throughout the island. Radon activities in the groundwater samples were determined following the procedure outlined by Savatier and Rocha [73] using a RAD-7/Rad H_2O monitor set to the "WAT250" protocol with corrections for the time elapsed between sampling and measurement.

SGD rates at each site were calculated at a 30-minute time step with a transient radon mass balance box model [74] using (a) measured radon inventories, corrected for a ~15 minute response delay [75], salinity and tidal stage data and (b) empirical corrections to account for radon losses (offshore mixing, atmospheric evasion, and radioactive decay) and gains (diffusion from the seabed sediment and from in-situ production from dissolved ^{226}Ra). Estimated SGD rates were converted into volumetric freshwater SGD fluxes using a groundwater radon endmember mean value of 1104 dpm L^{-1} (SD = 610 dpm L^{-}) derived from sampling of the aforementioned spring and 6 groundwater wells. Importantly, these estimates are representative for tidal cycles at single spot locations and not for study area-wide conditions captured by the 20 experimental samplers. Additionally, the applied groundwater radon end-member for the flux calculations may not capture local conditions at the individual surveys. However, the

strong correlation between concurrently measured radon and salinity data (e.g., Fig. S5) indicates salinity to be an adequate freshwater SGD tracer at the experimental sites.

Current speed and direction

We used an acoustic doppler current profiler (ADCP) to characterize the current velocity and direction during the sampling period. At each site, an upward-looking acoustic Doppler current profiler (ADCP) (Nortek Aquadopp Profiler HR 2MHz) was weighted and placed in a sand channel 5m from the nearest patch reef at a depth of 2m. The ADCP sampled from 0.15 to 1.0m above the seafloor for 60 seconds at 2 Hz every 2 or 10 minutes (depending on deployment length) for 2 to 4 days. We calculated current measurements by averaging all samples in a burst and averaging over the full depth to produce a Eulerian velocity time series of depth-averaged current speed (m/s) and direction. Dry season ADCP deployments in 2021 occurred August 4-6, 11-15, 21-24 (Varari) and August 8-10 (Cabral); wet season deployments in 2022 occurred March 21-27 (Varari) and March 29-31 (Cabral).

Ecosystem metabolism calculation

Ecosystem metabolism was calculated similarly to Silbiger et al. (2020) [15] using changes in TA and dissolved inorganic carbon (DIC). DIC was calculated from TA and pH (total) using the seacarb package [71]. The mean ± SE error propagation for the DIC calculation from TA (error of 5 μmol kg^{-1}) and pH (error of 0.01) is 7.62 ± 0.021 μmol kg^{-1}. To account for groundwater mixing, TA and DIC were first normalized to SiO_3^{2-}, a common tracer for SGD [15,66], using the following equation:

$$C_1 = C_{mix} + (C_{mix} - C_{SGD}) * (\frac{Si_{mic} - 0.965}{Si_{SGD} - Si_{mix}}),$$

Where C_1 is the SiO_3^{2-} - normalized TA or DIC concentration at the open-ocean reference value (0.965 μmol L^{-1}), C_{mix} is the measured TA or DIC value (SGD-marine mixture), C_{SGD} is the endmember TA or DIC value, Si_{mix} is the measured SiO_3^{2-} value (SGD-marine mixture) and Si_{SGD} is the average groundwater endmember (Table 1). The reference SiO_3^{2-} value was taken from a nearby offshore location from the Global Ocean Data Project [76].

NEC and NEP potential [77] were calculated for each sampling location × time point: NEC potential was calculated as ΔTA/2 and NEP potential was calculated as ΔDIC - ΔTA/2. ΔTA or ΔDIC is the difference between the SiO_3^{2-} - normalized TA or DIC concentration and the average offshore TA or DIC concentration collected at the reef crest. ΔTA was divided by two because 1 mol of $CaCO_3$ is produced per 2 mol of TA uptake [51]. NEC potential is subtracted from NEP potential to remove any carbon taken up or released from inorganic processes. Differences in TA or DIC are commonly used as a proxy for net calcification/production (TA or DIC depletion) or net dissolution/respiration (TA or DIC repletion) on coral reefs [15,77,78]. The terms NEC and NEP are used for brevity within this paper. We avoided calculating true NEC and NEP rates because both field sites are very shallow (< 2m) with a complex hydrodynamic environment, and small uncertainties in residence time calculations can lead to highly inaccurate ecosystem metabolism rates [79].

Statistical analyses

To characterize the composition of the SGD from the seepage point by each site and season, we calculated the Pearson's correlation coefficient of log-transformed values for each measured variable (TA, pH, temperature, humic fDOM, proteinaceous fDOM, N+N, NH_4^+, SiO_3^{2-}, PO_4^{3-}) as a function of salinity. To visualize how SGD affected reef biogeochemistry over diel, tidal, and season time frames, we used a principal components analysis on log-transformed values. The data were centered and standardized by season and individual PCAs were created for each site. To characterize the biogeochemical cascade created by SGD we developed individual Bayesian structural equation models (SEM) for each site and

season. Each SEM was based on a system of six equations, where each equation represents a set of hypotheses based on our current understanding of SGD and coral reef biology (Table 2; Fig. 4). All data used in the SEMs were centered and standardized and N+N and SiO_3^{2-} were log-transformed in all models to meet assumptions of normality. Bayesian models were run using the R package *brms* [80,81], which is based on the Hamiltonian Monte Carlo algorithm from STAN. To achieve model convergence, we ran three parallel chains of length 2000, with a warm-up of 1000, and a thinning parameter of 1. We used a multivariate normal distribution and all parameters had relatively uniform priors (student t distribution (d.f. = 3, $\mu = 0$, $\sigma = 10$)). We visually checked all trace plots and calculated Gelman-Rubin statistics [82] for all parameters to assess model convergence. Posterior predictive checks using the *pp_check* function in the *tidybayes* R package [83] were used to assess model fit. All results are reported as medians with two-tailed 95% Bayesian credible intervals. Effect sizes with credible intervals that do not overlap zero are considered to be statistically significant. All analyses were performed in the R statistical program [84]. All data and code are available on GitHub at https://github.com/njsilbiger/BiogeochemicalCascades_SGD and Zenodo [publicly available upon acceptance].

Acknowledgments

We thank the local residents at our two field sites and the current and past indigenous stewards of Mo'orea, French Polynesia for allowing us to conduct research on their land. In particular we thank T. Cabral, Flora, Juliette, and Bruno for graciously allowing us to work in their backyards. We thank the many field and lab hands for help with water collection and processing. The work was made possible with funding from NSF Biological Oceanography grants to NJS (#1924281), CEN and MJD (#1923877), and CEN (#1949033), an NSF Hydrological Sciences grant to BH (#1936671) as well as the NSF funded Mo'orea LTER (#1637396). Additional financial support to the MCR LTER was provided through a general gift from the Gordon and Betty Moore Foundation. Research was completed under permits issued by the French Polynesian Government (Délégation à la Recherche) and the Haut-commissariat de la République en Polynésie Française (DTRT) (Protocole d'Accueil 2005-2022).

References

1. Jefferies, R. L. Allochthonous inputs: integrating population changes and food-web dynamics. *Trends Ecol. Evol.* **15**, 19–22 (2000).
2. Polis, G. A., Anderson, W. B. & Holt, R. D. Toward an integration of landscape and food web ecology: The dynamics of spatially subsidized food webs. *Annu. Rev. Ecol. Syst.* **28**, 289–316 (1997).
3. Dayton, P. K., Tegner, M. J., Edwards, P. B. & Riser, K. L. Temporal and spatial scales of kelp demography: The role of oceanographic climate. *Ecol. Monogr.* **69**, 219–250 (1999).
4. Brown, T. A. *et al.* High contributions of sea ice derived carbon in polar bear (Ursus

558 maritimus) tissue. *PLoS One* **13**, e0191631 (2018).
559 5. Delevaux, J. M. S. *et al.* A linked land-sea modeling framework to inform ridge-to-reef
560 management in high oceanic islands. *PLoS One* **13**, e0193230 (2018).
561 6. Sandin, S. A. *et al.* Harnessing island–ocean connections to maximize marine benefits of
562 island conservation. *Proceedings of the National Academy of Sciences* **119**, e2122354119
563 (2022).
564 7. Graham, N. A. J. *et al.* Seabirds enhance coral reef productivity and functioning in the
565 absence of invasive rats. *Nature* **559**, 250–253 (2018).
566 8. Pastorok, R. A. & Bilyard, G. R. Effects of sewage pollution on coral-reef communities.
567 *Marine ecology progress series. Oldendorf* **21**, 175–189 (1985).
568 9. Dubinsky, Z. & Stambler, N. Marine pollution and coral reefs. *Glob. Chang. Biol.* **2**, 511–526
569 (1996).
570 10. Adam, T. C. *et al.* Landscape-scale patterns of nutrient enrichment in a coral reef
571 ecosystem: implications for coral to algae phase shifts. *Ecol. Appl.* **31**, e2227 (2021).
572 11. Silbiger, N. J. & Sorte, C. J. B. Biophysical feedbacks mediate carbonate chemistry in
573 coastal ecosystems across spatiotemporal gradients. *Sci. Rep.* **8**, 796 (2018).
574 12. Ricart, A. M. *et al.* Coast-wide evidence of low pH amelioration by seagrass ecosystems.
575 *Glob. Chang. Biol.* **27**, 2580–2591 (2021).
576 13. Lowe, A. T., Bos, J. & Ruesink, J. Ecosystem metabolism drives pH variability and
577 modulates long-term ocean acidification in the Northeast Pacific coastal ocean. *Sci. Rep.* **9**,
578 963 (2019).
579 14. Fields, J. B. & Silbiger, N. J. Foundation species loss alters multiple ecosystem functions
580 within temperate tidepool communities. *Mar. Ecol. Prog. Ser.* (2022)
581 doi:10.3354/meps13978.
582 15. Silbiger, N. J., Donahue, M. J. & Lubarsky, K. Submarine groundwater discharge alters

583 coral reef ecosystem metabolism. *Proc. Biol. Sci.* **287**, 20202743 (2020).

584 16. Silbiger, N. J. *et al.* Nutrient pollution disrupts key ecosystem functions on coral reefs. *Proc.*
585 *Biol. Sci.* **285**, 10.1098/rspb.2017.2718 (2018).

586 17. Bracken, M. E. S., Silbiger, N. J., Bernatchez, G. & Sorte, C. J. B. Primary producers may
587 ameliorate impacts of daytime CO2 addition in a coastal marine ecosystem. *PeerJ* **6**, e4739
588 (2018).

589 18. Kwiatkowski, L. *et al.* Nighttime dissolution in a temperate coastal ocean ecosystem
590 increases under acidification. *Sci. Rep.* **6**, 22984 (2016).

591 19. Cyronak, T., Schulz, K. G., Santos, I. R. & Eyre, B. D. Enhanced acidification of global coral
592 reefs driven by regional biogeochemical feedbacks. *Geophys. Res. Lett.* **41**, 5538–5546
593 (2014).

594 20. Wegley Kelly, L. *et al.* Distinguishing the molecular diversity, nutrient content, and energetic
595 potential of exometabolomes produced by macroalgae and reef-building corals. *Proc. Natl.*
596 *Acad. Sci. U. S. A.* **119**, (2022).

597 21. Quinlan, Z. A. *et al.* Fluorescent organic exudates of corals and algae in tropical reefs are
598 compositionally distinct and increase with nutrient enrichment. *Limnology and*
599 *Oceanography Letters* **3**, 331–340 (2018).

600 22. Haas, A. F. *et al.* Effects of coral reef benthic primary producers on dissolved organic
601 carbon and microbial activity. *PLoS One* **6**, e27973 (2011).

602 23. Goldberg, S. J., Nelson, C. E., Viviani, D. A., Shulse, C. N. & Church, M. J. Cascading
603 influence of inorganic nitrogen sources on DOM production, composition, lability and
604 microbial community structure in the open ocean. *Environ. Microbiol.* **19**, 3450–3464
605 (2017).

606 24. Lesser, M. P. Eutrophication on Coral Reefs: What Is the Evidence for Phase Shifts,
607 Nutrient Limitation and Coral Bleaching. *Bioscience* **71**, 1216–1233 (2021).

25. Santos, I. R. *et al.* Submarine groundwater discharge impacts on coastal nutrient biogeochemistry. *Nature Reviews Earth & Environment* **2**, 307–323 (2021).
26. Moosdorf, N., Stieglitz, T., Waska, H., Dürr, H. H., & Hartmann, J. Submarine groundwater discharge from tropical islands: a review. *Grundwasser* **20**, 53–67 (2015).
27. Nelson, C. E. *et al.* Fluorescent dissolved organic matter as a multivariate biogeochemical tracer of submarine groundwater discharge in coral reef ecosystems. *Mar. Chem.* **177**, 232–243 (2015).
28. Cyronak, T., Santos, I. R., Erler, D. V. & Eyre, B. D. Groundwater and porewater as major sources of alkalinity to a fringing coral reef lagoon (Muri Lagoon, Cook Islands). *Biogeosciences* (2013).
29. Paytan, A. *et al.* Submarine groundwater discharge: An important source of new inorganic nitrogen to coral reef ecosystems. *Limnol. Oceanogr.* **51**, 343–348 (2006).
30. La Valle, F. F., Kantar, M. B. & Nelson, C. E. Coral reef benthic community structure is associated with the spatiotemporal dynamics of submarine groundwater discharge chemistry. *Limnol. Oceanogr.* **n/a**, (2020).
31. La Valle, F., Thomas, F. I. M. & Nelson, C. E. Macroalgal biomass, growth rates, and diversity are influenced by submarine groundwater discharge and local hydrodynamics in tropical reefs. *Mar. Ecol. Prog. Ser.* 51–67 (2019).
32. Lubarsky, K. A., Silbiger, N. J. & Donahue, M. J. Effects of submarine groundwater discharge on coral accretion and bioerosion on two shallow reef flats. *Limnol. Oceanogr.* **63**, 1660–1676 (2018).
33. Amato, D. W., Smith, C. M. & Duarte, T. K. Submarine Groundwater Discharge Differentially Modifies Photosynthesis, Growth, and Morphology for Two Contrasting Species of Gracilaria (Rhodophyta). *Hydrology* **5**, 65 (2018).
34. Crook, E. D., Cohen, A. L., Rebolledo-Vieyra, M., Hernandez, L. & Paytan, A. Reduced

calcification and lack of acclimatization by coral colonies growing in areas of persistent natural acidification. *Proceedings of the National Academy of Sciences* **110**, 11044–11049 (2013).

35. Richardson, C. M., Dulai, H., Popp, B. N., Ruttenberg, K. & Fackrell, J. K. Submarine groundwater discharge drives biogeochemistry in two Hawaiian reefs. *Limnol. Oceanogr.* **62**, S348–S363 (2017).
36. Moore, W. S. The effect of submarine groundwater discharge on the ocean. *Ann. Rev. Mar. Sci.* **2**, 59–88 (2010).
37. Santos, I. R., Eyre, B. D. & Huettel, M. The driving forces of porewater and groundwater flow in permeable coastal sediments: A review. *Estuar. Coast. Shelf Sci.* **98**, 1–15 (2012).
38. Kleypas, J. A. & Langdon, C. Coral Reefs and Changing Seawater Carbonate Chemistry. in *Coral Reefs and Climate Change: Science and Management* 73–110 (American Geophysical Union, 2006).
39. Middelburg, J. J., Soetaert, K. & Hagens, M. Ocean Alkalinity, Buffering and Biogeochemical Processes. *Rev. Geophys.* **58**, e2019RG000681 (2020).
40. Wu, P., Christidis, N. & Stott, P. Anthropogenic impact on Earth's hydrological cycle. *Nature Climate Change* vol. 3 807–810 Preprint at https://doi.org/10.1038/nclimate1932 (2013).
41. Moosdorf, N. & Oehler, T. Societal use of fresh submarine groundwater discharge: An overlooked water resource. *Earth-Sci. Rev.* **171**, 338–348 (2017).
42. Haßler, K. *et al.* Provenance of nutrients in submarine fresh groundwater discharge on Tahiti and Moorea, French Polynesia. *Appl. Geochem.* **100**, 181–189 (2019).
43. Robertson, G. P. & Vitousek, P. M. Nitrogen in Agriculture: Balancing the Cost of an Essential Resource. *Annu. Rev. Environ. Resour.* **34**, 97–125 (2009).
44. Slomp, C. P. & Van Cappellen, P. Nutrient inputs to the coastal ocean through submarine groundwater discharge: controls and potential impact. *J. Hydrol.* **295**, 64–86 (2004).

45. McMahon, A. & Santos, I. R. Nitrogen enrichment and speciation in a coral reef lagoon driven by groundwater inputs of bird guano. *J. Geophys. Res. C: Oceans* **122**, 7218–7236 (2017).

46. Tamborski, J. *et al.* A comparison between water circulation and terrestrially-driven dissolved silica fluxes to the Mediterranean Sea traced using radium isotopes. *Geochim. Cosmochim. Acta* **238**, 496–515 (2018).

47. Dillon, P. J. & Kirchner, W. B. The effects of geology and land use on the export of phosphorus from watersheds. *Water Res.* **9**, 135–148 (1975).

48. Dulai, H., Smith, C. M., Amato, D. W., Gibson, V. & Bremer, L. L. Risk to native marine macroalgae from land-use and climate change-related modifications to groundwater discharge in Hawai‘i. *Limnol. Oceanogr. Lett.* **8**, 141–153 (2023).

49. Azam, F. *et al.* The Ecological Role of Water-Column Microbes in the Sea. *Marine Ecology Progress Series* vol. 10 257–263 Preprint at https://doi.org/10.3354/meps010257 (1983).

50. Johnson, E. E. & Wiegner, T. N. Surface water metabolism potential in groundwater-fed coastal waters of Hawaii island, USA. *Estuaries Coast.* **37**, 712–723 (2014).

51. Chisholm, J. R. M. & Gattuso, J.-P. Validation of the alkalinity anomaly technique for investigating calcification of photosynthesis in coral reef communities. *Limnol. Oceanogr.* **36**, 1232–1239 (1991).

52. Andersson, A. J. & Gledhill, D. Ocean acidification and coral reefs: effects on breakdown, dissolution, and net ecosystem calcification. *Ann. Rev. Mar. Sci.* **5**, 321–348 (2013).

53. Gattuso, J.-P., Frankignoulle, M. & Wollast, R. Carbon and carbonate metabolism in coastal aquatic ecosystems. *Annu. Rev. Ecol. Syst.* **29**, 405–434 (1998).

54. Johnson, A. G., Glenn, C. R. & Burnett, W. C. Aerial infrared imaging reveals large nutrient-rich groundwater inputs to the ocean. *Geophysical* (2008).

55. Santos, I. R., Glud, R. N., Maher, D. & Erler, D. Diel coral reef acidification driven by

683 porewater advection in permeable carbonate sands, Heron Island, Great Barrier Reef.
684 *Geophys. Res. Lett.* doi:10.1029/2010GL046053.
685 56. Courtney, T. A. *et al.* Environmental controls on modern scleractinian coral and reef-scale
686 calcification. *Sci Adv* **3**, e1701356 (2017).
687 57. Davis, K. L., Colefax, A. P., Tucker, J. P., Kelaher, B. P. & Santos, I. R. Global coral reef
688 ecosystems exhibit declining calcification and increasing primary productivity.
689 *Communications Earth & Environment* **2**, 1–10 (2021).
690 58. Silverman, J., Lazar, B. & Erez, J. Effect of aragonite saturation, temperature, and nutrients
691 on the community calcification rate of a coral reef. *J. Geophys. Res.* **112**, 1 (2007).
692 59. McDonough, L. K. *et al.* Changes in global groundwater organic carbon driven by climate
693 change and urbanization. *Nat. Commun.* **11**, 1279 (2020).
694 60. Nelson, C. E., Wegley Kelly, L. & Haas, A. F. Microbial Interactions with Dissolved Organic
695 Matter Are Central to Coral Reef Ecosystem Function and Resilience. *Ann. Rev. Mar. Sci.*
696 **15**, 431–460 (2023).
697 61. Luijendijk, E., Gleeson, T. & Moosdorf, N. Fresh groundwater discharge insignificant for the
698 world's oceans but important for coastal ecosystems. *Nat. Commun.* **11**, 1260 (2020).
699 62. Anthony, K. R. N., A. Kleypas, J. & Gattuso, J.-P. Coral reefs modify their seawater carbon
700 chemistry - implications for impacts of ocean acidification. *Glob. Chang. Biol.* **17**, 3655–
701 3666 (2011).
702 63. Hughes, T. P., Graham, N. A. J., Jackson, J. B. C., Mumby, P. J. & Steneck, R. S. Rising to
703 the challenge of sustaining coral reef resilience. *Trends Ecol. Evol.* **25**, 633–642 (2010).
704 64. McLaughlin, C. J., Smith, C. A., Buddemeier, R. W., Bartley, J. D. & Maxwell, B. A. Rivers,
705 runoff, and reefs. *Glob. Planet. Change* **39**, 191–199 (2003).
706 65. Odum, E. P. The strategy of ecosystem development. *Science* **164**, 262–270 (1969).
707 66. Oehler, T. *et al.* DSi as a Tracer for Submarine Groundwater Discharge. *Frontiers in Marine*

Science **6**, (2019).

67. Cyronak, T., Santos, I. R., Erler, D. V., Maher, D. T. & Eyre, B. D. Drivers of pCO2 variability in two contrasting coral reef lagoons: The influence of submarine groundwater discharge. *Global Biogeochem. Cycles* **28**, 2013GB004598 (2014).
68. Enochs, I. C. *et al.* Subsurface Automated Samplers (SAS) for ocean acidification research. *Bulletin of Marine Science* Preprint at https://doi.org/10.5343/bms.2020.0018 (2020).
69. Mos, B., Holloway, C., Kelaher, B. P., Santos, I. R. & Dworjanyn, S. A. Alkalinity of diverse water samples can be altered by mercury preservation and borosilicate vial storage. *Sci. Rep.* **11**, 9961 (2021).
70. Dickson, A. G. & Et, A. Guide to best practices for ocean CO2 measurement. Preprint at https://doi.org/10.25607/OBP-1342 (2007).
71. Gattuso, J.-P., Epitalon, J.-M., Lavigne, H. & Orr, J. seacarb: Seawater Carbonate Chemistry. R package version 3.2. 12. (2019).
72. Coble, P. G., Lead, J., Baker, A. & Reynolds, D. M. *Aquatic Organic Matter Fluorescence*. (Cambridge University Press, 2014).
73. Savatier, M. & Rocha, C. Rethinking tracer-based (Ra, Rn, salinity) approaches to estimate point-source submarine groundwater discharge (SGD) into coastal systems. *J. Hydrol.* **598**, 126247 (2021).
74. Burnett, W. C. & Dulaiova, H. Estimating the dynamics of groundwater input into the coastal zone via continuous radon-222 measurements. *J. Environ. Radioact.* **69**, 21–35 (2003).
75. Petermann, E. & Schubert, M. Quantification of the response delay of mobile radon-in-air detectors applied for detecting short-term fluctuations of radon-in-water concentrations. *Eur. Phys. J. Spec. Top.* **224**, 697–707 (2015).
76. Olsen, A. *et al.* The Global Ocean Data Analysis Project version 2 (GLODAPv2) – an internally consistent data product for the world ocean. *Earth Syst. Sci. Data* **8**, 297–323

(2016).

77. Cyronak, T. *et al.* Taking the metabolic pulse of the world's coral reefs. *PLoS One* **13**, e0190872 (2018).

78. Yeakel, K. L. *et al.* Shifts in coral reef biogeochemistry and resulting acidification linked to offshore productivity. *Proc. Natl. Acad. Sci. U. S. A.* **112**, 14512–14517 (2015).

79. Courtney, T. A. & Andersson, A. J. Evaluating measurements of coral reef net ecosystem calcification rates. *Coral Reefs* **38**, 997–1006 (2019).

80. Bürkner, P.-C. Advanced Bayesian multilevel modeling with the R package brms. The R Journal, 10 (1), 395-411. Preprint at (2018).

81. Bürkner, P. C. An R package for bayesian multilevel models using Stan. *J. Stat. Softw.*

82. Gelman, A. & Rubin, D. B. Inference from Iterative Simulation Using Multiple Sequences. *Stat. Sci.* **7**, 457–472 (1992).

83. Kay, M. *tidybayes: Tidy Data and Geoms for Bayesian Models*. (2018). doi:10.5281/zenodo.1308151.

84. R Core Team. R: A language and environment for statistical computing. https://www.R-project.org/. (2021).

Supplementary Files

This is a list of supplementary files associated with this preprint. Click to download.

- supplement.pdf